Ge/SiGe quantum confined Stark effect electro-absorption modulation with low voltage swing at $\lambda = 1550$ nm

D. C. S. Dumas,[1] K. Gallacher,[1] S. Rhead,[2] M. Myronov,[2] D. R. Leadley,[2] and D. J. Paul[1,*]

[1]*School of Engineering, University of Glasgow, Rankine Building, Oakfield Avenue, Glasgow, G12 8LT, UK*

[2]*Department of Physics, University of Warwick, Coventry, CV4 7AL, UK*

[*]*Douglas.Paul@glasgow.ac.uk*

Abstract: Low-voltage swing ($\leq$1.0 V) high-contrast ratio (6 dB) electro-absorption modulation covering 1460 to 1560 nm wavelength has been demonstrated using Ge/SiGe quantum confined Stark effect (QCSE) diodes grown on a silicon substrate. The heterolayers for the devices were designed using an 8-band **k**.**p** Poisson-Schrödinger solver which demonstrated excellent agreement with the experimental results. Modelling and experimental results demonstrate that by changing the quantum well width of the device, low power Ge/SiGe QCSE modulators can be designed to cover the S- and C-telecommunications bands.

OCIS codes: (230.4110) Modulators; (230.4205) Multiple quantum well (MQW) modulators; (230.0250) Optoelectronics; (230.2090) Electro-optical devices.

References and links

1. D. J. Paul, "Silicon photonics: a bright future?" Elec. Lett. **45**, 582–584 (2009).
2. D. A. B. Miller, "Device requirements for optical interconnects to silicon chips," Proc. IEEE **97**, 1166–1185 (2009).
3. G. T. Reed, G. Mashanovich, F. Y. Gardes, and D. J. Thomson, "Silicon optical modulators," Nature Photon. **4**, 518–526 (2010).
4. F. Morichetti, A. Canciamilla, C. Ferrari, A. Samarelli, M. Sorel, and A. Melloni, "Travelling-wave resonant four-wave mixing breaks the limits of cavity-enhanced all-optical wavelength conversion," Nature Comm. **2**, 296 (2011).
5. Q. Xu, B. Schmidt, S. Pradhan, and M. Lipson, "Micrometre-scale silicon electro-optic modulator," Nature **435**, 325–327 (2005).
6. D. J. Thomson, F. Gardes, J. M. Fedeli, S. Zlatanovic, Y. Hu, B. P. P. Kuo, E. Myslivets, N. Alic, S. Radic, G. Z. Mashanovich, and G. T. Reed, "50-Gb/s silicon optical modulator," IEEE Photon. Technol. Lett. **24**, 234–236 (2012).
7. J. Liu, M. Beals, A. Pomerene, S. Bernardis, R. Sun, J. Cheng, L. C. Kimerling, and J. Michel, "Waveguide-integrated, ultralow-energy GeSi electro-absorption modulators," Nature Photon. **2**, 433–437 (2008).
8. D. Feng, S. Liao, H. Liang, J. Fong, B. Bijlani, R. Shafiiha, B. J. Luff, Y. Luo, J. Cunningham, A. V. Krishnamoorthy, and M. Asghari, "High speed GeSi electro-absorption modulator at 1550 nm wavelength on SOI waveguide," Opt. Express **20**, 22224–22232 (2012).
9. Y. H. Kuo, Y. K. Lee, Y. S. Ge, S. Ren, J. E. Roth, T. I. Kamins, D. A. B. Miller, and J. S. Harris, "Strong quantum-confined Stark effect in germanium quantum-well structures on silicon," Nature **437**, 1334–1336 (2005).
10. E. H. Edwards, L. Lever, E. T. Fei, T. I. Kamins, Z. Ikonic, J. S. Harris, R. W. Kelsall, and D. A. B. Miller, "Low-voltage broad-band electroabsorption from thin Ge/SiGe quantum wells epitaxially grown on silicon," Opt. Express **21**, 867–876 (2013).
11. P. Chaisakul, D. Marris-Morini, J. Frigerio, D. Chrastina, M.-S. Rouifed, S. Cecchi, P. Crozat, G. Isella, and L. Vivien, "Integrated germanium optical interconnects on silicon substrates," Nature Photon. **8**, 482–488 (2014).

#213587 - $15.00 USD Received 9 Jun 2014; revised 24 Jul 2014; accepted 24 Jul 2014; published 1 Aug 2014

12. P. Chaisakul, D. Marris-Morini, M. S. Rouifed, J. Frigerio, G. Isella, D. Chrastina, J.-R. Coudevylle, X. L. Roux, S. Edmond, D. Bouville, and L. Vivien, "Strong quantum-confined Stark effect from light hole related direct-gap transitions in Ge quantum wells," Appl. Phys. Letts. **102**, 191107 (2013).
13. (http://www.nextnano.de/nextnano3/).
14. D. J. Paul, "The progress towards terahertz quantum cascade lasers on silicon substrates," Laser & Photon. Rev. **4**, 610–632 (2010).
15. D. J. Paul, "8-band **k**.**p** modeling of the quantum confined Stark effect in Ge quantum wells on Si substrates," Phys. Rev. B **77**, 155323 (2008).
16. D. A. B. Miller, D. S. Chemla, T. C. Damen, A. C. Gossard, W. Wiegmann, T. H. Wood, and C. A. Burrus, "Band-edge electroabsorption in quantum well structures: The quantum-confined Stark effect," Phys. Rev. Lett. **53**, 2173–2176 (1984).
17. S. Ren, Y. Rong, S. Claussen, R. Schaevitz, T. Kamins, J. Harris, and D. Miller, "Ge/SiGe quantum well waveguide modulator monolithically integrated with SOI waveguides," IEEE Photon. Technol. Letts. **24**, 461–463 (2012).
18. M. S. Rouifed, P. Chaisakul, D. Marris-Morini, J. Frigerio, G. Isella, D. Chrastina, S. Edmond, X. L. Roux, J.-R. Coudevylle, and L. Vivien, "Quantum-confined Stark effect at 1.3μm in Ge/$Si_{0.35}Ge_{0.65}$ quantum-well structure," Opt. Lett. **37**, 3960–3962 (2012).
19. E. H. Edwards, R. M. Audet, E. T. Fei, S. A. Claussen, R. K. Schaevitz, E. Tasyurek, Y. Rong, T. I. Kamins, J. S. Harris, and D. A. B. Miller, "Ge/SiGe asymmetric Fabry-Perot quantum well electroabsorption modulators," Opt. Express **20**, 29164–29173 (2012).
20. V. Shah, A. Dobbie, M. Myronov, and D. Leadley, "High quality relaxed Ge layers grown directly on a Si (001) substrate," Solid-State Electron. **62**, 189 – 194 (2011).
21. M. M. Mirza, H. Zhou, P. Velha, X. Li, K. E. Docherty, A. Samarelli, G. Ternent, and D. J. Paul, "Nanofabrication of high aspect ratio ($\sim$50:1) sub-10 nm silicon nanowires using inductively coupled plasma etching," J. Vac. Sci. Technol. B **30**, 06FF02 (2012).
22. K. Gallacher, P. Velha, D. J. Paul, I. MacLaren, M. Myronov, and D. R. Leadley, "Ohmic contacts to n-type germanium with low specific contact resistivity," Appl. Phys. Letts. **100**, 022113 (2012).
23. M. Vanecek and A. Poruba, "Fourier-transform photocurrent spectroscopy of microcrystalline silicon for solar cells," Appl. Phys. Letts. **80**, 719–721 (2002).
24. R. Schaevitz, J. Roth, S. Ren, O. Fidaner, and D. Miller, "Material properties of Si-Ge/Ge quantum wells," IEEE J. Select. Topics Quantum Elec. **14**, 1082–1089 (2008).
25. P. Chaisakul, D. Marris-Morini, G. Isella, D. Chrastina, X. L. Roux, E. Gatti, S. Edmond, J. Osmond, E. Cassan, and L. Vivien, "Quantum-confined Stark effect measurements in Ge/SiGe quantum-well structures," Opt. Lett. **35**, 2913–2915 (2010).
26. Semiconductor Industry Association, "International technology roadmap for semiconductors," Tech. rep., Semiconductor Industry Association (2013).

1. Introduction

The bandwidth of data transferred between microprocessors, memory and hard or solid state disks in most supercomputer and desktop computer systems is now limited by the high cost of increasing the number of copper input/output channels beyond the present densities. The point has therefore been reached where optical interconnects can provide higher bandwidth but the key for adoption is the ability to find a suitable cost effective optical technology which can be mass manufactured [1]. Si photonics is one such technology that is presently being pursued but such optical interconnects at the chip scale have strict requirements in terms of energy consumption, voltage swing, bandwidth, and monolithic integration [2] that must be obtained if the technology is to succeed.

Modulators [3] are a key requirement for most Si photonics applications and many different types of Si photonics modulators have been demonstrated using heaters [4], Si p-i-n modulators [5, 6] and the Franz-Keldysh effect [7, 8]. One of the Si photonic modulators that can meet all the requirements for monolithically integrated Si photonics modulators is based on the quantum confined Stark effect (QCSE) using Ge/SiGe multiple quantum wells (MQWs) [2, 3, 9]. Ge/SiGe MQWs have shown electro-absorption modulation over the telecommunications bands [10]. Ge/$Si_{0.19}Ge_{0.81}$ QCSE MQW devices with five QWs grown on $Si_{0.12}Ge_{0.88}$ have been demonstrated contrast ratios of around 5 dB in the S- (1460 - 1530 nm) and C- (1530 - 1565 nm) telecommunications bands for a 1 V swing with up to 3.3 V applied [10]. QCSE

#213587 - $15.00 USD Received 9 Jun 2014; revised 24 Jul 2014; accepted 24 Jul 2014; published 1 Aug 2014

modulators integrated with Ge waveguides and photodetectors have also recently been realised [11].

In this work an 8-band **k**.**p** Poisson-Schrödinger tool is used to design compact $Ge/Si_{0.15}Ge_{0.85}$ MQWs for p-i-n diode QCSE electro-absorption modulation devices for low voltage operation. QCSE devices with improved contrast ratios of 6 dB above previous values [10] with only 1 V of swing at 1.55 μm are demonstrated through the higher substrate Ge content, tensile strain from the virtual substrate, an increase in the number of QWs and the reduction in spacer thickness. These effects combine to move the absorption edge to longer wavelength and to reduce the required applied voltage swing for low power operation at 1.55 μm. Whilst the present results are demonstrated experimentally with surface-normal measurements (TE polarization, electric field parallel to the QW plane), the **k**.**p**-modelling also demonstrates that such MQW designs will operate at similar wavelengths for TM polarized light (electric field normal to the QW plane) in waveguide geometry devices which can support both TE and TM light. This opens up the potential for novel operation schemes for modulation using both polarisations [12].

2. Design and simulation

The absorption spectra, wavefunctions, and energy levels of the MQW structure were calculated using an 8-band **k**.**p** tool available through NEXTNANO [13]. The designs rely on ten Ge QWs and eleven $Si_{0.18}Ge_{0.82}$ barriers all grown to be strain symmetrized on top of thin virtual substrates grown on Si (001) substrates thereby allowing structures far thicker than the critical thickness limitations [14]. For the calculation it was assumed that the structure was fully strained to a $Si_{0.04}Ge_{0.96}$ relaxed buffer region with 0.10% to 0.30% residual tensile strain [15]. The material parameters used for all the calculations are those from reference [15]. The computational complexity of simulating the full structure with ten QWs and a suitable number of subband and $k_{||}$ states for even a single design and applied voltage was prohibitive with the available computational resources so the wavefunctions and absorption spectrum were calculated for a single QW. For the QW widths and barrier thicknesses there is overlap between wave functions in adjacent QWs which perturbs the calculated results. As will be demonstrated in the work, the perturbation is small enough that the tool is able to design with sufficient accuracy to allow a full understanding of the experimental results.

The absorption edge of a QCSE device is modulated by increasing the bias applied to the device (Fig. 1). An increase in the reverse bias applied across the QWs moves the absorption edge between confined conduction and valence subband states inside the Ge QW to lower energies while decreasing the height of the absorption peak [16]. The electron and hole wavefunctions in the QWs are shifted in opposite directions in space while moving closer together in energy (Fig. 1(a)) resulting in the absorption moving to longer wavelengths. It is this change in absorption as a function of wavelength as the voltage is increased that is used to build a modulator device. The devices are generally operated in reverse bias, but a small forward bias (lower than the built in bias) can also be used to allow the devices to operate with very low dark currents.

The absorption edge for a given applied bias can be controlled by changing either the strain in the growth (Fig. 1(b)) or the QW width (Fig. 2). Modelling of the QW width (Fig. 2) indicates that 6.6 nm wide Ge QWs are appropriate for parts of the E- (1360 - 1460 nm) and S-telecoms bands whilst an 11 nm (11.3 $\pm$ 0.3 nm grown) or 13.6 $\pm$ 0.3 nm Ge QW should allow both S- and C-band operation. From the simulations, Fig. 1(b) demonstrates that when the tensile strain in the buffer layer is increased (which increases the lattice constant on which the QWs epilayers are grown), the absorption edge shifts to lower energies with the light-hole 1 (LH1) energy level shifting faster relative to the Γ-valley subband 1 (Γ1) than the heavy-hole 1 (HH1) energy level. Fig. 1 demonstrates that the tensile strain moves the LH band to higher electron

#213587 - $15.00 USD Received 9 Jun 2014; revised 24 Jul 2014; accepted 24 Jul 2014; published 1 Aug 2014

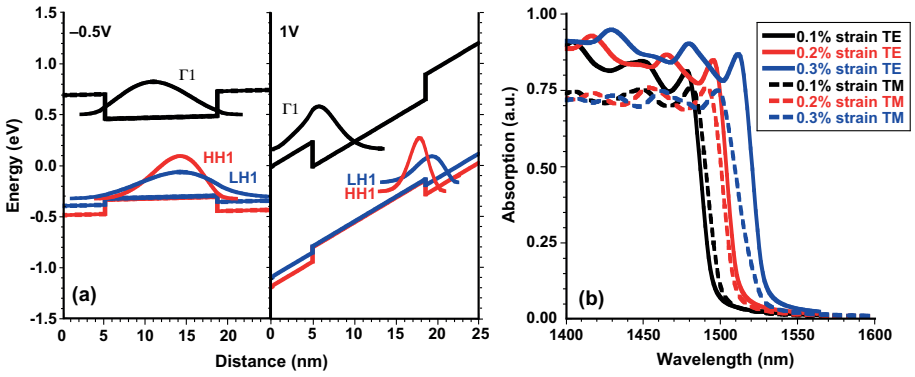

Fig. 1. (a) The calculated wavefunctions for Γ1, HH1 and LH1 of a 13.6 nm wide Ge QW at applied bias voltages of -0.5 V (left) and 1 V (right) for 0.2% tensile strain. As the applied bias is increased the hole and electron energy levels move closer together and the overlap of the wavefunctions decreases. (b) The calculated absorption spectrum from single QW simulations for a 13.6 nm QW QCSE device with $Si_{0.18}Ge_{0.82}$ barriers on a strained $Si_{0.04}Ge_{0.96}$ buffer layer for different levels of tensile strain for TE and TM polarizations.

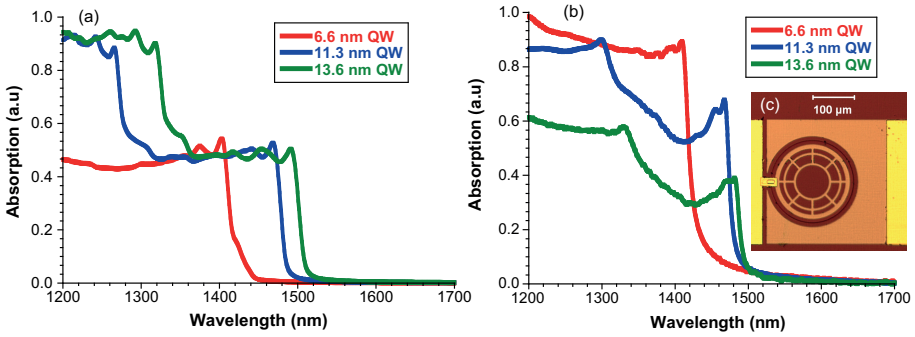

Fig. 2. (a) The calculated absorption spectra for a single quantum well for the three structures grown with Ge QWs and $Si_{0.18}Ge_{0.82}$ barriers on $Si_{0.04}Ge_{0.96}$ virtual substrates. (b) The measured experimental absorption for the same three QW widths. (c) An optical microscope image of the top spider contact on top of the photodetector device used for measurements.

energy (lower hole energy) so it becomes comparable in energy to the HH state resulting in the absorption edges for the TE and TM polarizations being at the same wavelength. This indicates that the absorption at 0.1 and 0.2 % tensile strain are close to polarization independent so that devices will have similar operational wavelengths for both TE and TM-polarization. There are two competing effects on the energy of the absorption edge from increasing the QW width; the states in the QW reduce in energy and the lowering of the electric field across the QWs for a given bias. As the QW width is increased, the subband states in the QWs move closer together and decrease the absorption energy for creating an electron-hole pair while the increase in the total width of the device increases the energy of the absorption edge through a reduction in the build-in electric field of the p-i-n junction. The overall effect for these designs is a decrease in the energy (increase in wavelength) of the absorption edge as the QW width is increased as is demonstrated by the modelling in Fig. 2(a).

Three wafers with different MQW regions were designed and grown with the widths of the

#213587 - $15.00 USD Received 9 Jun 2014; revised 24 Jul 2014; accepted 24 Jul 2014; published 1 Aug 2014

Table 1. The layer thickness as extracted by TEM and the composition extracted by XRD for the three designed wafers.

Wafer	Ge QW width	Barrier width	Barrier	Buffer
1	6.6 ± 0.3 nm	8.2 nm $\pm$ 0.4	$Si_{0.18}Ge_{0.82}$	$Si_{0.04}Ge_{0.96}$
2	11.3 ± 0.3 nm	11.5 nm $\pm$ 0.4	$Si_{0.18}Ge_{0.82}$	$Si_{0.04}Ge_{0.96}$
3	13.6 ± 0.3 nm	12.5 nm $\pm$ 0.4	$Si_{0.18}Ge_{0.82}$	$Si_{0.04}Ge_{0.96}$

QWs (barriers) from 6.6 nm (8.2 nm), to 13.6 nm (12.5 nm) aiming to cover the E-, S- and C-telecommunication bands. Thinner barriers require a lower applied voltage for a given electric field across the QWs, and increases the effective absorption coefficient due to a higher density of QWs per active region. The present designs used a larger Ge QW contribution to the space in the active region in an attempt to increase the absorption (for the 11 nm QW, 66 % of the Ge/SiGe MQW stack is Ge QWs by design which was reduced to 50 % when grown - see Table 1). This Ge QW contribution to space in the active region is higher than the 37 % - 43 % [10, 17, 18, 19] in other published designs.

3. Growth and fabrication

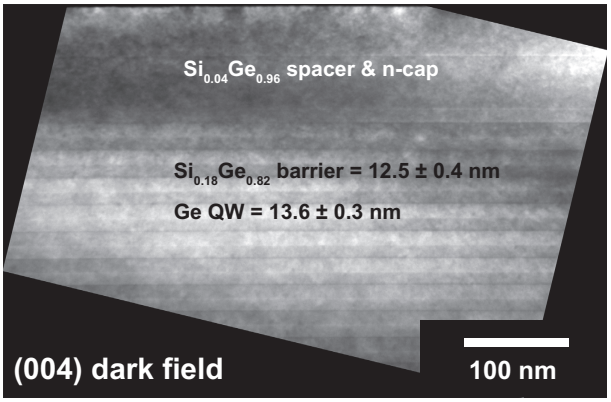

Fig. 3. A TEM image showing the Ge cap and top spacer then the $Si_{0.18}Ge_{0.82}$ barriers and Ge QWs closest to the surface of the wafer for the sample with the widest QWs.

The MQW structures were grown on Si wafers using an ASM Epsilon 2000E low pressure chemical vapor deposition tool [20] with silane, germane, diborane and phosphine. A 1 μm thick Ge seed layer was first deposited on a Si(001) wafer followed by a 250 nm thick reverse graded Si_xGe_{1-x} from $x = 0$ to $x = 0.04$ buffer. Next a virtual substrate of 500 nm thick $Si_{0.04}Ge_{0.96}$ layer was grown. The actual thicknesses of the layers were measured by cross-sectional transmission electron microscopy (TEM) shown in Fig. 3. The relaxation and composition was measured by x-ray diffraction (XRD) using reciprocal space maps (not shown). The Ge seed layer was measured to be 104.5 % relaxed relative to the Si(001) substrate, the $Si_{0.04}Ge_{0.96}$ buffer layer was 100 % relaxed relative to the Ge seed layer and the active layers were fully strained to the $Si_{0.04}Ge_{0.96}$ buffer. The residual strain in the Ge and $Si_{0.04}Ge_{0.96}$ layers is therefore $\sim$0.18% tensile strain.

The MQW structure designs consisted of a bottom contact layer of 400 nm p-type $Si_{0.04}Ge_{0.96}$ followed by a 50 nm i-$Si_{0.04}Ge_{0.96}$ spacer all grown at 400 ^{o}C. Next the MQW region, consisting of 11 barriers and 10 QWs of $Si_{0.18}Ge_{0.82}$ and Ge, respectively. This was fol-

#213587 - $15.00 USD Received 9 Jun 2014; revised 24 Jul 2014; accepted 24 Jul 2014; published 1 Aug 2014

lowed by a 50 nm i-$Si_{0.04}Ge_{0.96}$ spacer then a 50 nm n-type $Si_{0.04}Ge_{0.96}$ top contact layer doped with phosphorus. The measured layer thicknesses and Si content of SiGe layers in the as grown structure are presented in table 1. The TEM images in Fig. 3 indicate that all the heterolayers are flat and uniform without any significant buckling due to residual strain from the buffer or heterostructure layers.

To measure the actual absorption of the wafers as grown, photodiode devices were fabricated from each of the wafers. Each wafer was cleaved into 15 mm^2 samples on which circular diodes of 100 μm radius with spider web top contacts were fabricated (Fig. 2(c)). The circular mesas were created by photolithography and dry etched using a low-damage fluorine chemistry process [21]. Top and bottom Ohmic contacts were patterned simultaneously using a single photomask pattern. Ni was deposited and annealed to form low specific contact resistivity NiGe Ohmic contacts to the top n-type and bottom p-type heterolayers [22]. A 200 nm layer of silicon nitride was deposited for passivation and as an anti-reflection coating (ARC) on top of the etched device. In order to create electrical connects to the devices, via holes were etched and 10 nm Ti with 300 nm Al bond pads were deposited. The devices were initially tested using a probe station, then selected devices were wire-bonded to leadless chip carriers for optical characterisation in a Fourier transform infrared (FTIR) spectrometer. The current-voltage characteristics of the devices demonstrated good rectifying behaviour, with breakdown voltages greater than 5 V in reverse bias, corresponding to an electric field of at least 150 kV/cm.

4. Optical characterisation and analysis

The photocurrent spectrum as a function of bias voltage was measured for each sample using unpolarized light at normal incidence at 293 K. The diodes were positioned in the sample chamber of a Bruker Vertex 70 FTIR and characterized using a tungsten near-infrared source and a CaF_2 beamsplitter. In contrast to the standard FTIR setup which uses a commercial photodetector to measure the transmitted light, the photocurrent from the device under test was used as the measured signal for the FTIR [23]. A lock-in amplifier and a mechanical chopper were used to allow step-scan measurements which eliminates the dark current from measurements. The FTIR was then used to convert the time domain signal into the frequency domain. This technique has been demonstrated to be more sensitive than the more common direct transmission / absorption results that measures the photocurrent from a separate detector [23]. All measurements were surface-normal and therefore xy- or TE-polarized indicating that the Γ-valley to HH absorption is allowed whilst the Γ-valley to LH absorption is forbidden in the parabolic band approximation [15].

Fig. 2(b) provides the FTIR absorption experimental results for the three different QW widths at 293 K and 0 V bias. The experimental results agree extremely well with the simulations from the 8-band $\mathbf{k}.\mathbf{p}$ simulations. The simulations have not been scaled to account for the different % thicknesses of absorption material as the Ge QW widths have been changed over the ten QWs and this is why all the levels of absorption are similar in the simulations but not in the experimental results. The absorption edges from the simulations are close to the experimental values and certainly sufficient to understand the physical mechanisms in the devices. It is clear that to produce higher accuracy from the simulations, further analysis is required to understand any perturbations from the interactions of overlapping wavefunctions from adjacent QWs or differences in the experimental QW widths or residual strain from the original designs.

Although the FTIR allowed measurement of the photocurrent spectrum over a large bandwidth (Fig. 2(b)), the absolute value for the absorption coefficients could not be calculated from the photocurrent since the incident optical power at each wavelength was not known. In order to obtain values for the absorption coefficient, therefore, a tunable laser source (TLS) setup was used to measure the photocurrent of the devices. The TLS was set to 0.20 mW of output

#213587 - $15.00 USD Received 9 Jun 2014; revised 24 Jul 2014; accepted 24 Jul 2014; published 1 Aug 2014

power, which was directed through a lensed fibre and aligned at normal incidence to the diode. The fibre was aligned with micro-manipulators by maximising the photocurrent at 0.4 V applied bias and at 1460 nm wavelength. The photocurrent was then measured as a function of the applied bias and the wavelength. The laser wavelength was stepped between each current measurement, and then the applied voltage was stepped between each full wavelength sweep. The TLS allowed measurements over a narrow wavelength range (1460 to 1560 nm) and therefore was unable to measure the peak photocurrent of the 6.6 nm QW diodes. The output power from the lensed fibre was measured as a function of wavelength and the Fresnel reflection at the ARC was calculated to determine the maximum power reaching the QWs.

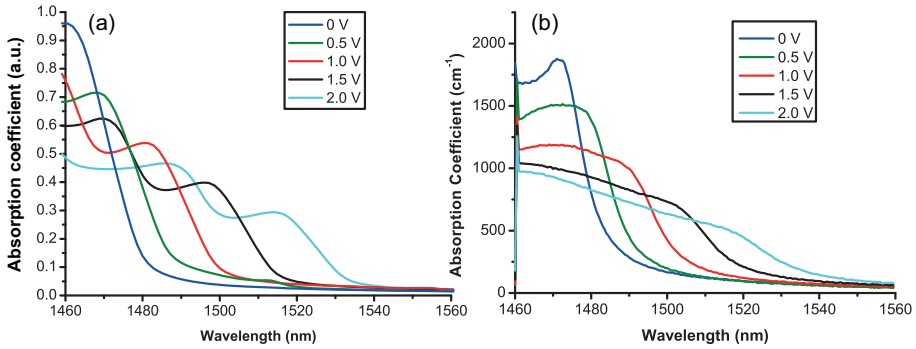

Fig. 4. (a) The calculated absorption spectra for the 11.3 nm QW device at applied bias voltages from 0 V to 3 V. (b) The experimental absorption coefficients as a function of applied reverse bias for the 11.3 nm Ge QW QCSE diodes as measured with a TLS.

The experimental absorption coefficient as a function of applied reverse bias was obtained using the following procedure and compared to the simulated spectra in Fig. 4(a). The calculated reflectance from the ARC at these wavelengths is 1.2 % and the output power was measured every 10 nm. Using a reflection loss of 1.2 % and interpolating from the calibrated output powers, the absorption coefficient for each wavelength and applied bias was then calculated from the TLS measurements and is shown in Fig. 4(b). The maximum absorption coefficient was at 0 V bias for the 11.3 nm Ge QW device and the peak photocurrent, after subtracting the dark current, was 6.17 μA at 1471 nm. Assuming that each electron in the photocurrent is due to one photon being absorbed, 4.4 % of the photons leaving the fibre lens are absorbed equating to an minimum absorption coefficient of 1875 cm^{-1} at 1471 nm. This is an improvement over previously reported absorption figures of 1600 cm^{-1} at 1450 nm using a similar number of ten QWs of 17 nm thickness with 40 nm thick barriers [24] but lower than the lower wavelength results at 1410 nm with an absorption of $\sim$3000 cm^{-1} using fifty Ge QWs of 10 nm thickness with 15 nm thick barriers [25]. The simulated spectrum in Fig. 4(a) agrees well with the experimental spectrum in Fig. 4(b). Whilst the agreement between experiment and simulations is good, it is not perfect as no account of the contact or access resistances has been included in this analysis and so further work is required to get complete agreement between simulations and experiment. The good agreement between simulations and experiment indicates the total access resistance in these devices is small.

Two of the key parameters for high performance modulators is the contrast ratio and the switching power which is dependent on the voltage swing of the device. Reducing the voltage swing is essential for low power operation but this voltage also has to be compatible with modern CMOS processes which presently use supply voltages around 1 V [26]. The simulated and experimentally measured contrast ratios as a function of applied and swing bias are presented in Fig. 5 for the 11.3 nm Ge QW device. There are small differences to the wavelength behaviour

#213587 - $15.00 USD Received 9 Jun 2014; revised 24 Jul 2014; accepted 24 Jul 2014; published 1 Aug 2014

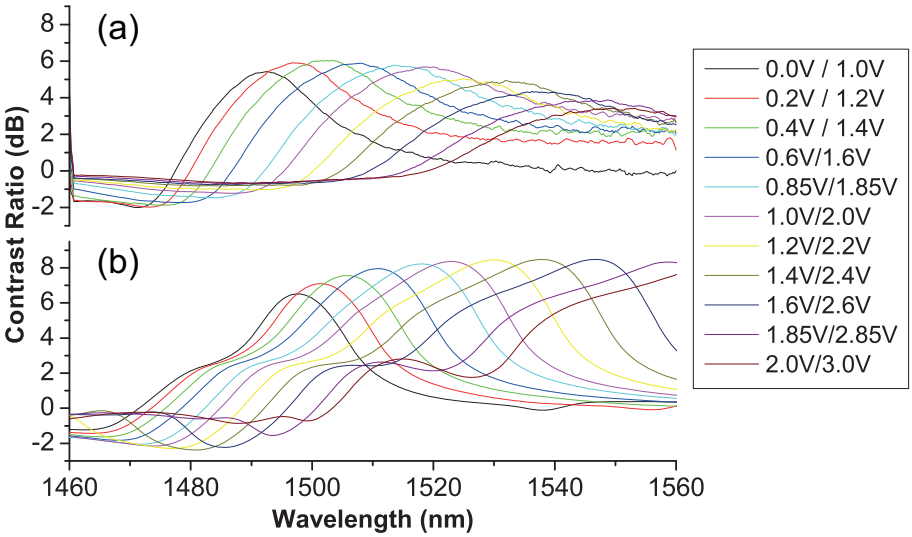

Fig. 5. (a) The experimentally measured contrast ratio for the 11.3 nm Ge QW device with a voltage swing of 1.0 V for bias voltages from 0.0 V to 2.0 V.(b) The calculated contrast ratio for a single 11.3 nm Ge QW simulation of the QCSE structure. The bias voltages was swept from 0 V to 2 V with a swing voltage of 1.0 V.

between the simulations and the experiment for a set of fixed voltages due to no account of the contact and access resistances being taken. It is also clear from the modelling that the interactions of the wavefunctions in adjacent QWs does not significantly change the operational wavelength of the device suggesting further reductions in the heterolayer barrier thicknesses could be used to further increase the contrast ratio by increasing the percentage of absorption material in the active layers. The 1 V swing photocurrent absorption contrast ratio is over 6 dB at 1495 nm for 0 V dc bias and decreases down to 4.0 dB at 1550 nm for 1.85 V dc bias (Fig. 5). From 1485 nm to 1520 nm in order to achieve at least 3 dB contrast ratio only a 0.3 V swing is required, a 0.4 V swing extends the 3 dB range to 1460 nm to 1535 nm. Compared to [10] this device has a higher contrast ratio at a 1 V swing, a lower applied dc bias and a lower voltage swing requirement for a 3 dB contrast ratio whilst simultaneously having an increased absorption of at least 1875 cm^{-1} compared to 1600 cm^{-1} in [10].

Whilst the experimental results presented are for a surface normal device, the simulations in Fig. 1 indicate that the present results are close to being polarization independent. This indicates that waveguide coupled devices will have nominally identical modulation as a function of the same applied bias at similar wavelengths. This suggests that waveguide coupled electro-absorption modulators based on the QCSE with a 1 V swing can be achieved using the same design of MQWs if grown on a suitable substrate for waveguides such as silicon-on-insulator thereby enabling QCSE devices for low power modulators in Si photonic technology.

5. Conclusions

To conclude, an 8-band **k**.**p** calculation using a single QW region was able to model the absorption edge for QCSE devices with thin barriers. QCSE electro-absorption modulation devices using Ge QWs separated by thin barriers were designed and fabricated. These reduced operating power designs demonstrated electro-optical modulation with lower applied voltage, lower voltage swing and higher absorption than previous designs at the important telecommunica-

#213587 - $15.00 USD Received 9 Jun 2014; revised 24 Jul 2014; accepted 24 Jul 2014; published 1 Aug 2014

tions S- and C-bands. At present the results are for surface-normal devices but the simulations indicate that the same heterolayer designs will operate at similar wavelengths in waveguide geometry devices. The results also indicate that the present interactions between wave functions in adjacent QWs is not significant and reduction in the heterolayer barrier thicknesses should further enhance the contrast ratios of the devices without significantly changing the operational wavelengths.

Acknowledgments

The authors would like to thank the staff of the James Watt Nanofabrication Centre for help with fabrication and Dr Marc Sorel for help in using the tunable laser. The work was funded by U.K. EPSRC.

#213587 - $15.00 USD Received 9 Jun 2014; revised 24 Jul 2014; accepted 24 Jul 2014; published 1 Aug 2014